Acta Polytechnica **64**(6):550–570, 2024
https://doi.org/10.14311/AP.2024.64.0550

Published by the Czech Technical University in Prague

SIMULATION OF WIND FLOW AROUND AN ALTERNATIVE FLAT-ROOFED FORTRESS TOWER RUIN

Martin Poliak[a,*], Michal Franek[b], Jana Gregorová[a]

[a] *Slovak University of Technology, Faculty of Civil Engineering, Department of Architecture, Radlinského 11, 810 05 Bratislava, Slovak Republic*

[b] *Slovak University of Technology, Faculty of Civil Engineering, Department of Building Construction, Radlinského 11, 810 05 Bratislava, Slovak Republic*

[*] corresponding author: martin.poliak@stuba.sk

Abstract. An analysis of the effects of alternative flat roof sizes and positions on wind flow around a ruin model is presented. The modelled ruin has almost cube-like proportions, with an open roof plane and a destroyed corner. Roofs over ruins are seen as a means of protection against the wind, which is considered a destructive mechanism. The purpose of the roof as a monumental means of presentation and limits of its implementation are also discussed. Wind flow is illustrated by external pressure and skin friction coefficients. Taking their changes into account, the degree of protection flat roof alternatives provide is estimated and optimal flat roof alternatives are discussed. Simulations were carried out using the 3D Time Steady Reynolds-averaged Navier-Stokes equations and the Shear Stress Transport k-ω turbulence model.

Keywords: Ruin protection, wind flow simulation, computational fluid dynamics, ruin coverage.

1. Introduction

A functional object is usually brought to a degraded state by the combined action of a spectrum of destructive mechanisms. Wind is one of the primary sources of natural destructive mechanisms of both a gradual and sudden nature [1, 2], of a mechanical, or chemical nature. It acts as a distributor and catalyst of other destructive mechanisms, such as water saturation and surface abrading by wind-driven sand [2–4]. The illustration of its behaviour around the protected structure also helps in the discussion of the effectiveness of the design of protective cover structures.

Ruins, as objects in an advanced stage of destruction, are among the objects highly sensitive to the mechanism effects and their further development caused by climate change [3]. This sensitivity is caused by the complexity of their geometry, caused both by the colourful morphology of the original object and by devastation, which creates complicated geometric systems. The sensitivity is also caused by the quality of the building material, used in the construction, or by its degradation, loosening and increasing its roughness, and porosity [5].

A roofed ruin, as a combination of the remains of an object in various stages of destruction and a roof structure of a certain shape and construction-material design, is a topic of a discussion by a group of concerned persons and professions. If the ruin is protected as a monument, the two ambitions of the given group will become paramount – an effective methodical monument presentation based on the available research results and its permanent technological and structural security. The entropic nature of any ruinous context limits the indisputable answer to both issues. This invites the continuation of the discussion and research of equally theoretical starting points for monument presentation and effective technical solutions for the protection of the material essence.

If the priority is to present historical values, the roof's dominant position should be allowed only if accurate information about the original roof in a particular period of the building's development are available. As soon as this information is missing, the preserved and stabilised ruin becomes the bearer of the presented values, which by this act becomes the next construction phase. The acknowledgement of this stage in subsequent additions rationalises the use of new formations, subordinate to the ruin and not reflecting any stages of previous development. When the focus is on protecting the ruin fabric, the roof is considered as an effective measure of passive protection. Its long-term use is rarely discussed in Czecho-Slovak context and its creation is usually due to other-than-protective reasons, possibly for easy possibility of contradiction with ruin's presentation requirements. However, a roof design with an overhang over the ruin's surface is deemed more effective and commonly used, usually as a temporary measure securing research and preceding traditional structure conservation. Water and its impact on the protected structure is a common topic of discussion in the management of ruin's protection, wind action as such is rarely considered for its unpredictive behaviour and difficult and time-consuming assessment. This study aims to contribute to this discussion and to the topic of roofing the ruins as a long-term solution.

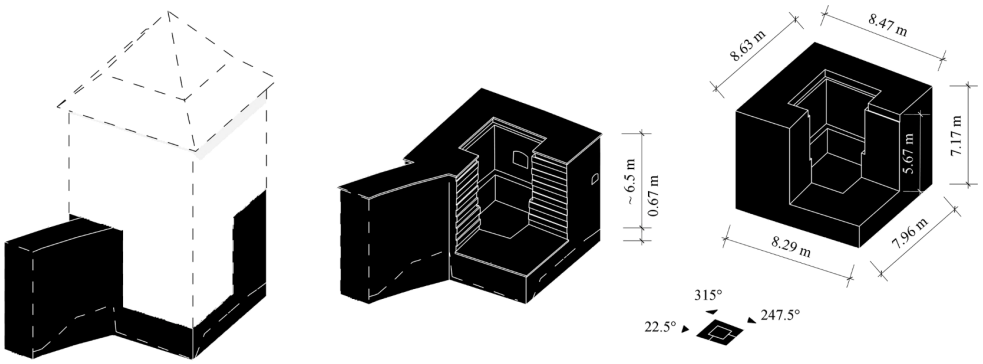

FIGURE 1. Model idealisation of the Trnava fortification tower, with simulated wind flow directions on the right bottom corner.

The geometry of a roofed ruin is determined by the geometry of the ruin itself as well as the geometry of the roof. The geometry of the ruin is closely related to the typology of the original object and the degree of its destruction. Roof geometry is related to the position of the roof in relation to the ruin, according to which roofs are divided into typologies – covering structures over the ruins or their entire site, protective structures with roof structures laid directly on the ruins, and protective structures with roof structures inserted into the ruins, the so-called containers [6, 7]. The morphology of the roof is a result of the differentiation and combination of the architectural characteristics of the roof structure itself, as well as of the distance from the ruin, if the roof is not directly laid on it.

The degree to which ruins are exposed to wind is closely related to the geometry of the resulting object. In terms of architectural design, the effects can be seen in changes in proportion, changes in shape, and the creation of architectural and structural details in the contact zone between the roof structure and the ruin [8–11]. From a purely geometric point of view, two parameters are of interest when analysing the geometry of the roof's contact with the ruin – in the vertical direction, the height of the roof installation, respectively its distance from the ruin, and in the horizontal direction, the size of the overlap of the roof in front of the face of the ruin, respectively the size of the embedding behind its face. There are two roof height limits that need to be considered. A preserved ruin's height is the limit within which a roofing installation should be set in the interest of presenting the ruin as a dominant part in the presentation methodology. The second height is the original roof height, if that information can be located through historical structure research.

The present article follows on from considerations that have examined the effectiveness of covering structures over ruins in order to protect them from deterioration [12–15]. In addition, it analyses the effectiveness of structures placed directly on the ruin as a means of protection, illustrating this with the aid of a wind study of flow changes caused by a specific variant of roofing. From a philosophical and methodological point of view, it relies on studies that are thematically similar [16, 17], considering monument material as a backbone of culturally and ecologically sustainable development and genius loci [18], reflected in different spatial scales and origins [19–23]. In doing so, it uses an idealised model of the ruin of the south-eastern corner tower of the Trnava fortifications that was previously identified as high cultural value location, currently undergoing stabilisation of method of its presentation [24], and as one of the potential climatically vulnerable locations [25]. Its various roofing solutions were analysed from an architectural-monumental point of view [26, 27]. From a wide range of possible geometric and structural solutions for the roof of the ruin, it chose a flat roof over the ruin, a characteristic compromise between the effort to protect the ruin structure and the intention of minimising interference with the architectural context.

2. Materials and methods

The presented ruin of the south-eastern corner tower of the city fortifications in Trnava, located near the city amphitheatre. Currently, it forms an open object with an almost square base with an approximate side length of 8.5 m and a height of approximately 6.5 m. The thickness of the masonry is not constant along the height, the locations of the former ceiling structures are indicated by thinning, so the thickness of the masonry reaches approximately 2.6 m at the base and 2 m at the head. Due to the destruction of the inner corner of the building, the ground plan footprint of the building can be roughly interpreted as the letter C. The remains of the eastern curtain of the fortification connect to the tower from the north. The two structures are of the same height. On the masonry heads, a thin concrete slab is mounted with a slight overlap to protect the masonry head from weathering.

In this and previous work, the current state of the tower has been idealised and some urban and architectural features have been abstracted in Figure 1. A plane was used to replace the diverse terrain configuration related to the presentation of this section

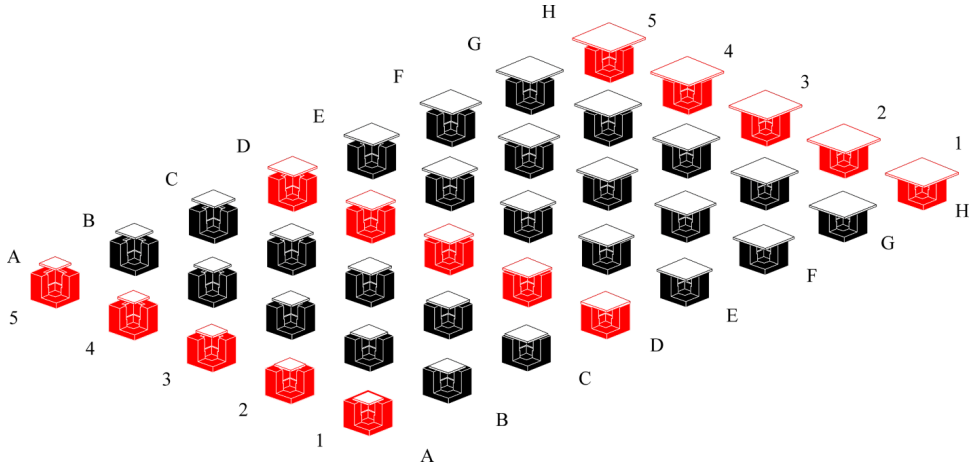

Figure 2. Matrix of considered roofs, alternating the height and overhang of the new roof, simulated branches of roofing alternatives marked in red.

of the fortification on the exterior rampart. The surrounding buildings, as well as greenery, which would interfere with the run-up area of the flow, were not considered. Similarly, the eastern curtain on the north side of the tower was also ignored, which made the building free-standing. Thus, a general situation was created with the aim of generalising boundary conditions and increasing the applicability of the observed changes in wind action and impact, caused precisely by manipulating the parameters of the roof covering structure. Moreover, the architectural details were abstracted, unique for the particular tower – such as the overhang of the concrete protective plate, the gunshot holes, the characteristic toothing of the masonry faces of the destroyed corner, and the difference in surface roughness between locations where different building materials were used was excluded as well.

The effect of a specific roof variant on the wind flow around a ruin is determined by observing two aspects of the roof-ruin relationship – the offset between the roof and the ruin (height of the spacer) and the size of the roof overlap, which can also be negative in size and set behind the ruin's masonry face. The characteristic dimension of the gradation between the two relationships was chosen as a quarter of the masonry thickness, in this case 0.5 m. This dimension is significant in architectural scale and is assumed to cause considerable changes in the monitored values of wind action. The extreme values of the roof overlap are 1.5 m behind the face of the masonry (branch A) and 2.0 m in front of the face (branch H), with offsets ranging from absolute contact (branch 1) to 2 m (branch 5). Board bodies representing a simplified flat roof geometry have a thickness of 0.5 meters. Based on the matrix of alternatives, a grid has been formed, which scales the overlap size in the direction of alternatives A–H, and the offset size from the ruin in the direction of alternatives 1–5 in Figure 2. Thus, the conventional design variants of covering roofs with overhang are simulated, while architectural approaches with finer, more subtle details are also being tested.

The experimental investigations were carried out in Boundary Layer Wind Tunnels (BLWT), where atmospheric circulation is simulated. Special devices, such as grids, foils and walls were used along the wind tunnel. The BLWT wind tunnel in Bratislava was designed with open-circuit scheme and two test sections. All the tests were conducted in the rear working section 2.6 m wide, 1.6 m high, and with 15 m long boundary layer (BL) simulation. 2.4 m diameter turntable allows to investigate different directions of incoming wind. The operating wind speed range is from 0.2 to 32 m s^{-1}. The mean wind velocity and intensity of turbulence profiles were simulated with plastic foil and a 150 mm wall. The BL simulations proved to be in good agreement with logarithmic law. The BL simulation with a value of roughness length $z_0 = 0.7$ m is between terrain categories III and IV. A 1:200 scale model have been selected for the study. Pneumatic transducer DSA 3217 made by Scanivalve was used to synchronously measure wind pressure on the principal building. This transducer had 16 individual, temperature compensated, piezoresistive pressure sensors, an A/D converter, and a microprocessor. Measuring process consisted of vinyl tubes, a circular pneumatic connector, and a pressure scanner with a rate of 500 samples/chan/sec. Pressure coefficients were developed from continuous sampling at about 500 samples per second over a period of about 30 s, corresponding to 39 min length in the full scale. Reference velocity was measured with Hot Wire Anemometry, MiniCTA 54T42 with a miniature wirestraight probe, type 55P11 from Dantec Dynamics. A static pitot tube was used to measure static pressure.

The wind flow simulations were performed using ANSYS Fluent software. The dimensions of the computational domain were $2.6 \times 1.6 \times 4.8$ m and were based on the maximum dimension of the idealised model [28] in a scale that was previously used in the calibration of the computational procedure by comparing the results of the exterior pressure coefficient $c_{pe,\mathrm{mean}}$ with experimental measurements. The com-

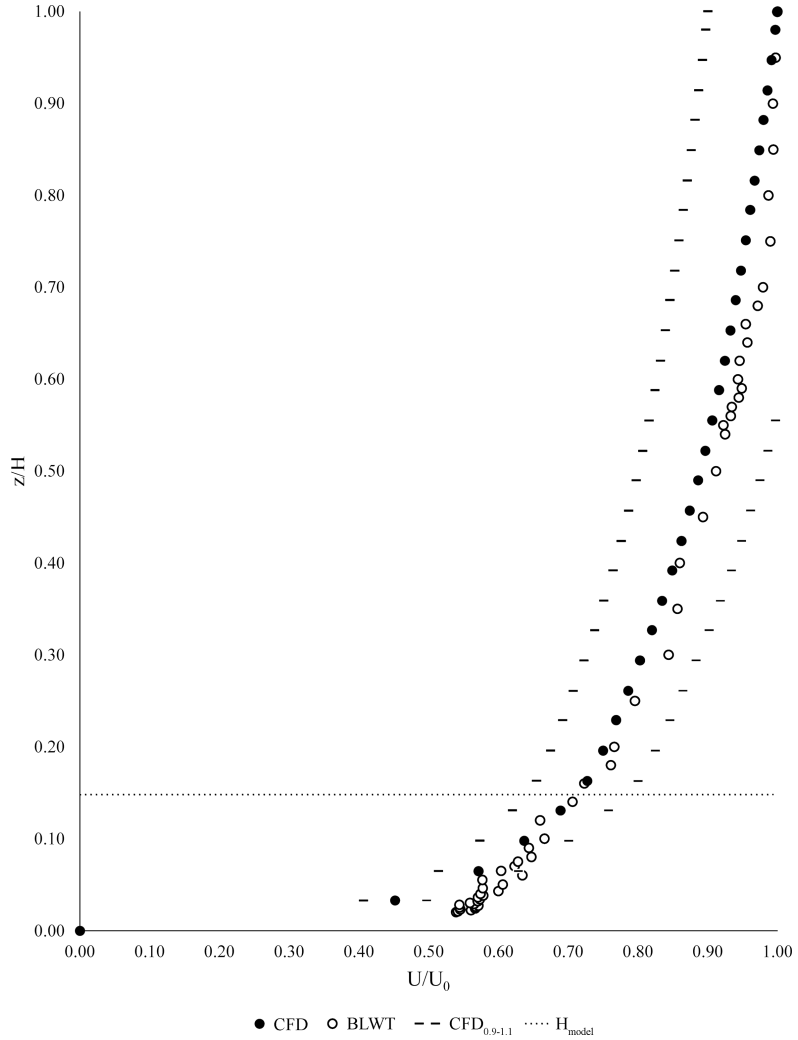

FIGURE 3. Flow velocity $\frac{U}{U_0}$ profiles obtained by calculation in CFD and experimental measurement in BLWT.

putational mesh was polyhedral with Growth Rate and Sizing limited to 1.1, with the assignment of Smooth Transition Inflation conditions for the first five layers above the terrain surface, and First Layer Thickness Inflation for the first five layers with a thickness of the first layer of 1 mm and a Sizing of 1 mm for the surface of the idealised ruin model, as well as the roofing. The numbers of mesh nodes ranged from 1.67 to 2.92 million and elements from 6.04 to 10.85 million (different rotations of the model when simulating multiple wind flow directions and different roof alternatives produced different numbers of mesh nodes and elements). There was a logarithmic wind profile with an aerodynamic roughness length of 0.7 m at the full scale set for the input area, symmetry with zero gradients for the top and side planes of the computational domain, uniform roughness of 0.5 mm height and 0.5 roughness constant for the ruin model, and 0.7 roughness constant for the terrain surface of 1.79 mm height. Reynolds-averaged Navier-Stokes Shear Stress Transport k-ω calculation model was chosen and flow simulations were performed as pressure based, time steady with no production limiter, and curvature correction, with max residue value set to 10^{-5}. Experimental and CFD results obtained using the given turbulence model and internal settings were in sufficient agreement,as can be seen in Figures 3, and 4, [29].

From the roof alternatives matrix, three branches were selected and simulated – A and H with minimum and maximum roof overlap, and middle branch D with no roof overlap and identical footprints for the roof and the ruin, as can be seen in Figure 2. Based on previous work [29], wind flows were simulated in three selected directions. The values of the exterior pressure coefficient c_{pe} and the surface friction coefficient c_f were monitored, given by the equations:

$$c_{pe} = \frac{p - p_s}{\frac{1}{2}\rho_0 . v_{ref}^2}, \tag{1}$$

$$c_f = \frac{\tau_w}{\frac{1}{2}\rho_0 . v_{ref}^2}, \tag{2}$$

where

p local static pressure [Pa],

p_s free stream mean static pressure [Pa],

ρ air density [kg m^{-3}],

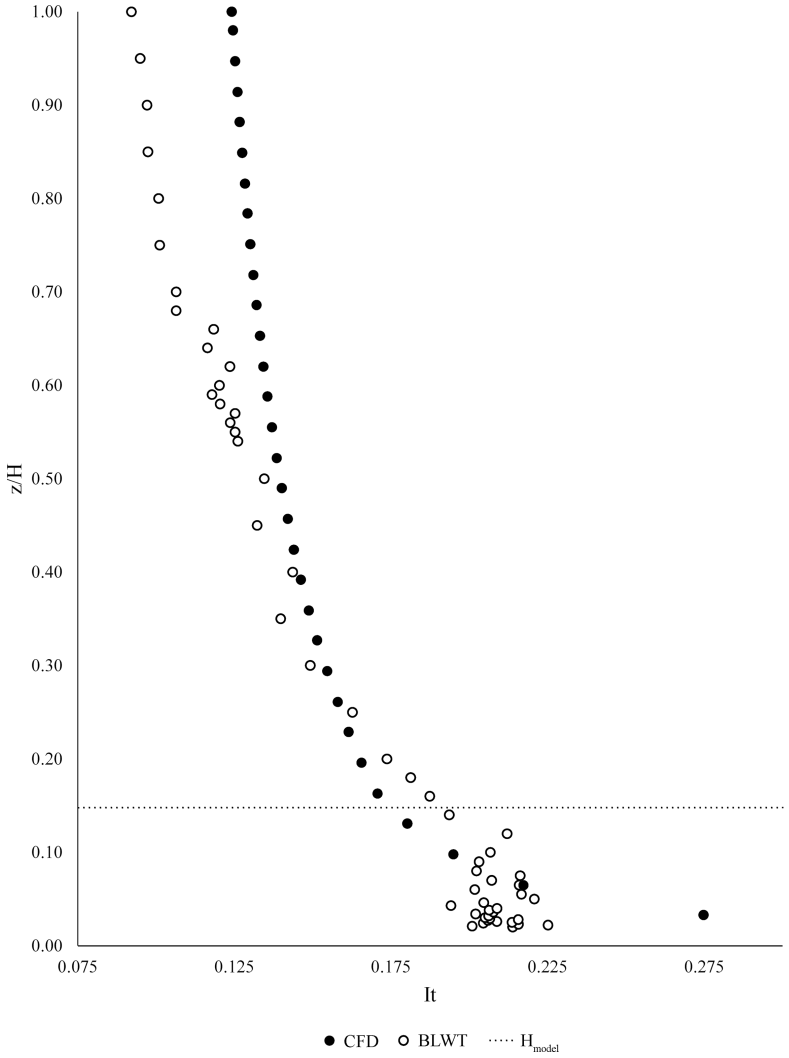

FIGURE 4. Turbulence intensity I_t profiles obtained by calculation in CFD and experimental measurement in BLWT.

v_{ref} reference wind flow velocity [$\mathrm{m\,s^{-1}}$], which was $13.616\,\mathrm{m\,s^{-1}}$,

τ_w local shear stress [Pa] [8, 30].

In the results post-processor, the position of the reference point in the calculation domain determines the values of both monitored coefficients. All simulated alternatives had the same position of this point set at the highest roofing alternative's height.

The mean values of the monitored coefficients were observed separately on the surfaces of the masonry head, exposed to high negative pressure values, the windward side (WW or short in tables), the most exposed to positive pressure, the leeward side (LW), and on the entire surface (ES) of the ruin model for the overall illustration of the protection of the ruin by the roof variant, see Table 1. The values were compared with those obtained flow around the ruin model without a roof, see Tables 2, 3 and 4. To assess the impact of individual roofing alternatives, the three differences in the observed coefficients obtained by simulating flow in three selected directions were averaged, see Table 5. The impact of other roofing alternatives, located on the unselected branches of the alternative matrix in Figure 2, was estimated by interpolation.

3. RESULTS

Figure 5 shows a histogram of mean changes in $c_{pe,\mathrm{mean}}$ values on the entire ruin model surface, grouped by roof overhang size from smallest to largest from roof alternative branch A to branch H. The most significant change within individual branches A–H was achieved by roof alternative 1, indicating that roof alternatives with direct contact with the ruin have the greatest impact on $c_{pe,\mathrm{mean}}$ values, which decrease with increasing distance from the ruin. The A1 roofing alternative disturbs this impression. When the roof in alternatives 2–5 is set at a certain distance from the ruin, however, the induced changes follow the expected pattern. Increasing values of the changes between the individual branches A–H indicate a direct relationship between the roofing overlap size and the change size. Roof alternative H1, i.e. roofing with the largest overlap in direct contact with the ruin, showed the largest change in $c_{pe,\mathrm{mean}}$ +0.099 (−39.5 %).

	$c_{pe,\mathrm{mean},22.5°}$				$c_{pe,\mathrm{mean},247.5°}$				$c_{pe,\mathrm{mean},315°}$			
	Head	**WW**	**LW**	**ES**	**Head**	**WW**	**LW**	**ES**	**Head**	**WW**	**LW**	**ES**
-	−0.601	0.151	−0.485	−0.327	−0.601	0.159	−0.486	−0.33	−0.657	0.302	−0.4	−0.187
A1	−0.631	0.165	−0.432	−0.286	−0.605	0.17	−0.434	−0.286	−0.575	0.319	−0.381	−0.151
A2	−0.502	0.175	−0.427	−0.272	−0.503	0.185	−0.427	−0.273	−0.502	0.315	−0.368	−0.147
...												
H4	−0.595	0.159	−0.443	−0.297	−0.541	0.189	−0.385	−0.251	−0.499	0.328	−0.374	−0.145
H5	−0.614	0.157	−0.461	−0.311	−0.609	0.163	−0.458	−0.31	−0.527	0.321	−0.371	−0.149

TABLE 1. A partial table with $c_{pe,\mathrm{mean}}$ values for three selected flow directions. See appendices for full table (Table 6).

	$c_{pe,\mathrm{mean},22.5°,\mathrm{diff}} = c_{pe,\mathrm{mean},22.5°,N} - c_{pe,\mathrm{mean},22.5°}$							
	Head		**Windward**		**Leeward**		**Entire Surface**	
A1	−0.03	5 %	0.015	10 %	0.053	−11 %	0.041	−13 %
A2	0.099	−17 %	0.024	16 %	0.058	−12 %	0.054	−17 %
...								
H3	0.058	−10 %	0.018	12 %	0.077	−16 %	0.059	−18 %
H4	0.006	−1 %	0.009	6 %	0.042	−9 %	0.029	−9 %
H5	−0.013	2 %	0.006	4 %	0.024	−5 %	0.016	−5 %

TABLE 2. A partial table with whole and percentage differences between the $c_{pe,\mathrm{mean}}$ values on the surface of the alternatively roofed ruin model and model without roof for flow direction 22.5°. See appendices for full table (Table 7).

	$c_{pe,\mathrm{mean},247.5°,\mathrm{diff}} = c_{pe,\mathrm{mean},247.5°,N} - c_{pe,\mathrm{mean},247.5°}$							
	Head		**Windward**		**Leeward**		**Entire Surface**	
A1	−0.004	1 %	0.011	7 %	0.052	−11 %	0.043	−13 %
A2	0.098	−16 %	0.026	16 %	0.06	−12 %	0.056	−17 %
...								
H4	0.06	−10 %	0.03	19 %	0.101	−21 %	0.079	−24 %
H5	−0.007	1 %	0.004	2 %	0.029	−6 %	0.019	−6 %

TABLE 3. A partial table with whole and percentage differences between the $c_{pe,\mathrm{mean}}$ values on the surface of the alternatively roofed ruin model and model without roof for flow direction 247.5°. See appendices for full table (Table 8).

	$c_{pe,\mathrm{mean},315°,\mathrm{diff}} = c_{pe,\mathrm{mean},315°,N} - c_{pe,\mathrm{mean},315°}$							
	Head		**Windward**		**Leeward**		**Entire Surface**	
A1	0.083	−13 %	0.017	6 %	0.019	−5 %	0.036	−19 %
A2	0.155	−24 %	0.013	4 %	0.031	−8 %	0.04	−21 %
...								
H4	0.159	−24 %	0.026	9 %	0.025	−6 %	0.042	−22 %
H5	0.131	−20 %	0.019	6 %	0.028	−7 %	0.038	−20 %

TABLE 4. A partial table with whole and percentage differences between the $c_{pe,\mathrm{mean}}$ values on the surface of the alternatively roofed ruin model and model without roof for flow direction 315°. See appendices for full table (Table 9).

$c_{pe,\mathrm{mean,mean\_diff}} = \frac{c_{pe,\mathrm{mean},22.5°,N} + c_{pe,\mathrm{mean},247.5°,N} + c_{pe,\mathrm{mean},315°}}{3}$	Head		Windward		Leeward		Entire Surface	
A1	0.16	−2 %	0.014	7 %	0.041	−9 %	0.04	−15 %
A2	0.18	−19 %	0.021	12 %	0.05	−11 %	0.05	−18 %
...								
H4	0.75	−12 %	0.022	11 %	0.056	−12 %	0.05	−18 %
H5	0.37	−6 %	0.01	4 %	0.027	−6 %	0.024	−10 %

TABLE 5. A partial table with mean differences of $c_{pe,\mathrm{mean}}$ values on the surface of the alternatively roofed ruin model and model without roof. See appendices for full table (Table 10).

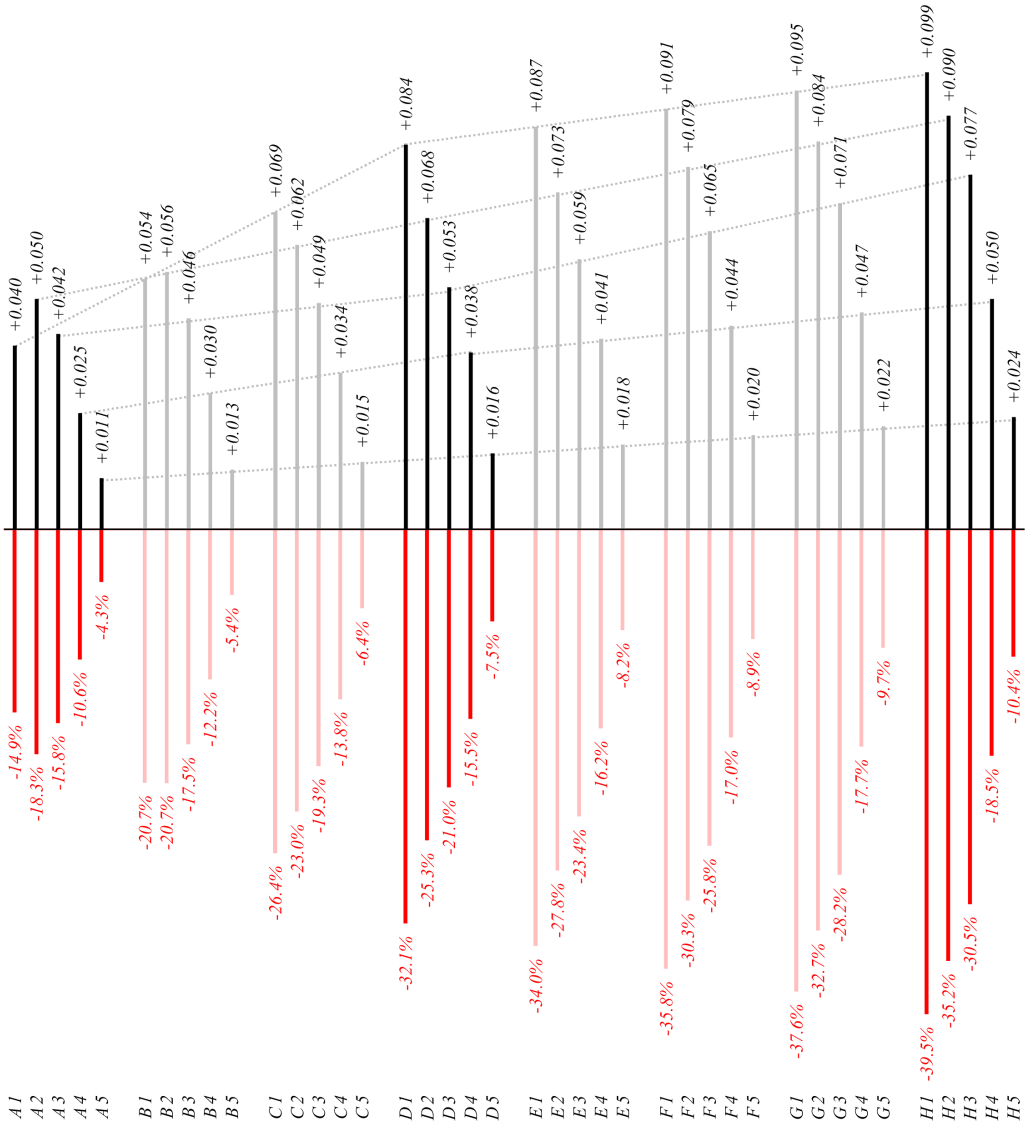

FIGURE 5. Histogram of mean changes in $c_{pe,\mathrm{mean}}$ on the entire surface of ruin model.

Figure 6 shows a histogram of mean changes in $c_{pe,\mathrm{mean}}$ values on the ruin masonry head. The largest monitored change (−100 %) represents the roof covering the head completely. Similarly, the monitored changes follow a similar pattern of dependency as the values monitored across the entire surface – larger changes are induced by closer roofing alternatives with a larger overlap. The second greatest value of change $c_{pe,\mathrm{mean}}$ +0.197 (−31.2 %) is observed by alternative H2, i.e. roofing with the largest overlap, 0.5 m away from the ruin.

Figure 7 shows a histogram of mean changes in $c_{pe,\mathrm{mean}}$ values on windward surfaces of the ruin model. Except for the difference between A1 and A2, where A2 roofing alternatives without direct contact with the ruin result in greater changes, they show similar development patterns. Changes monitored for the most distant roof alternatives 5 are close to negligible.

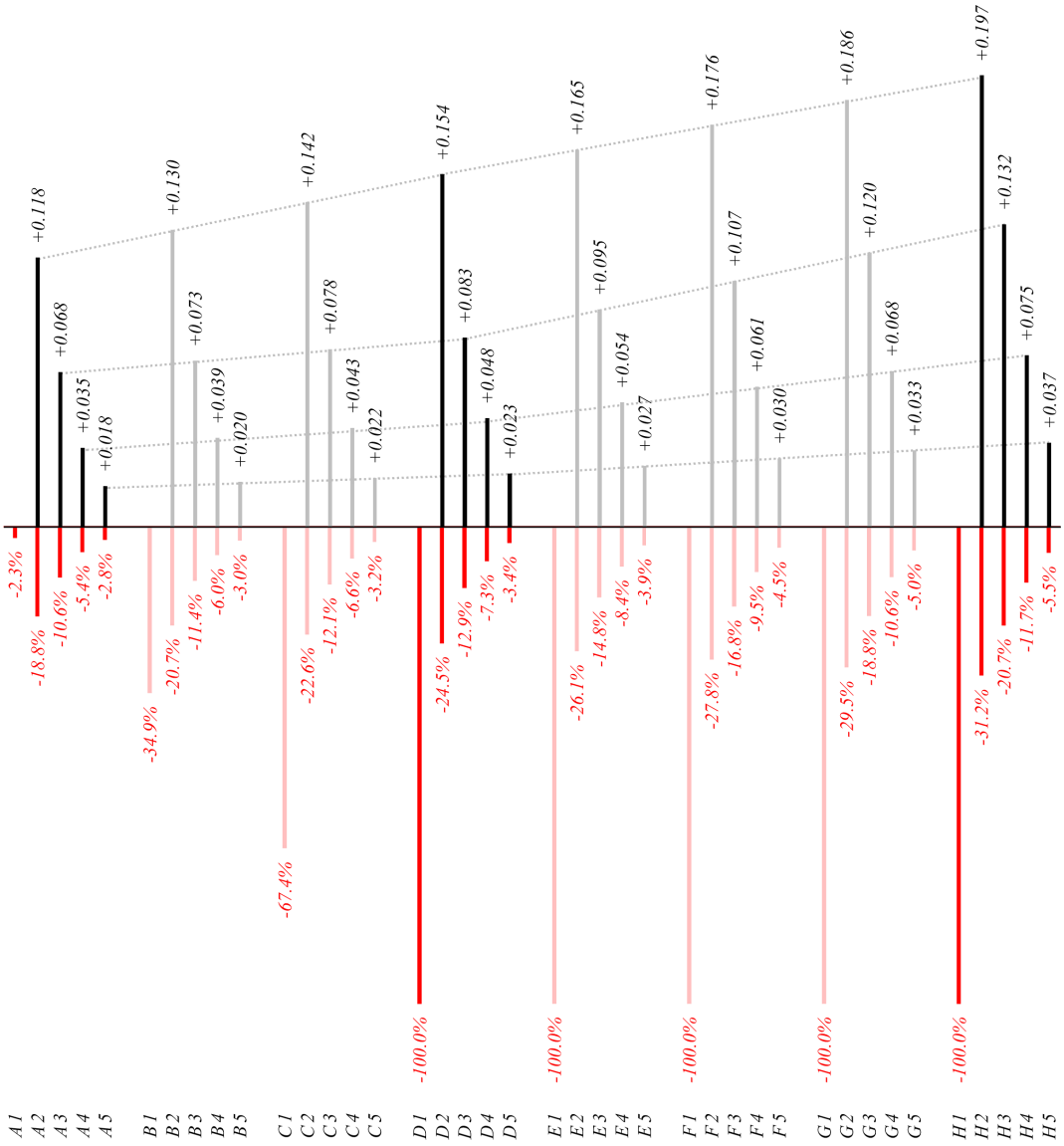

FIGURE 6. Histogram of mean changes in $c_{pe,\mathrm{mean}}$ on the ruin masonry heads.

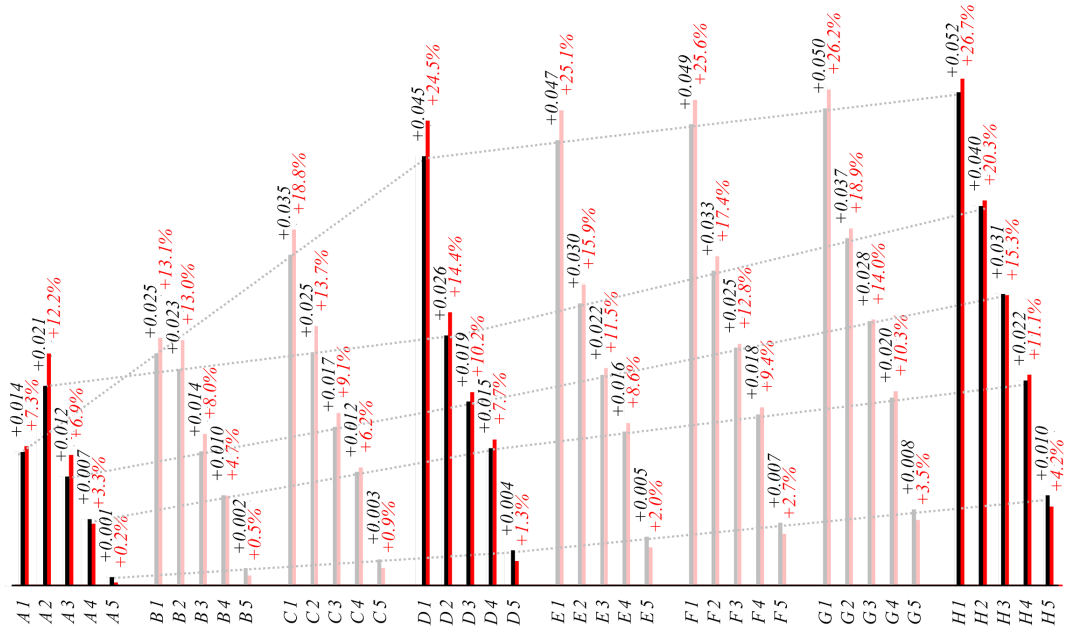

FIGURE 7. Histogram of mean changes in $c_{pe,\mathrm{mean}}$ on the windward faces of the ruin model.

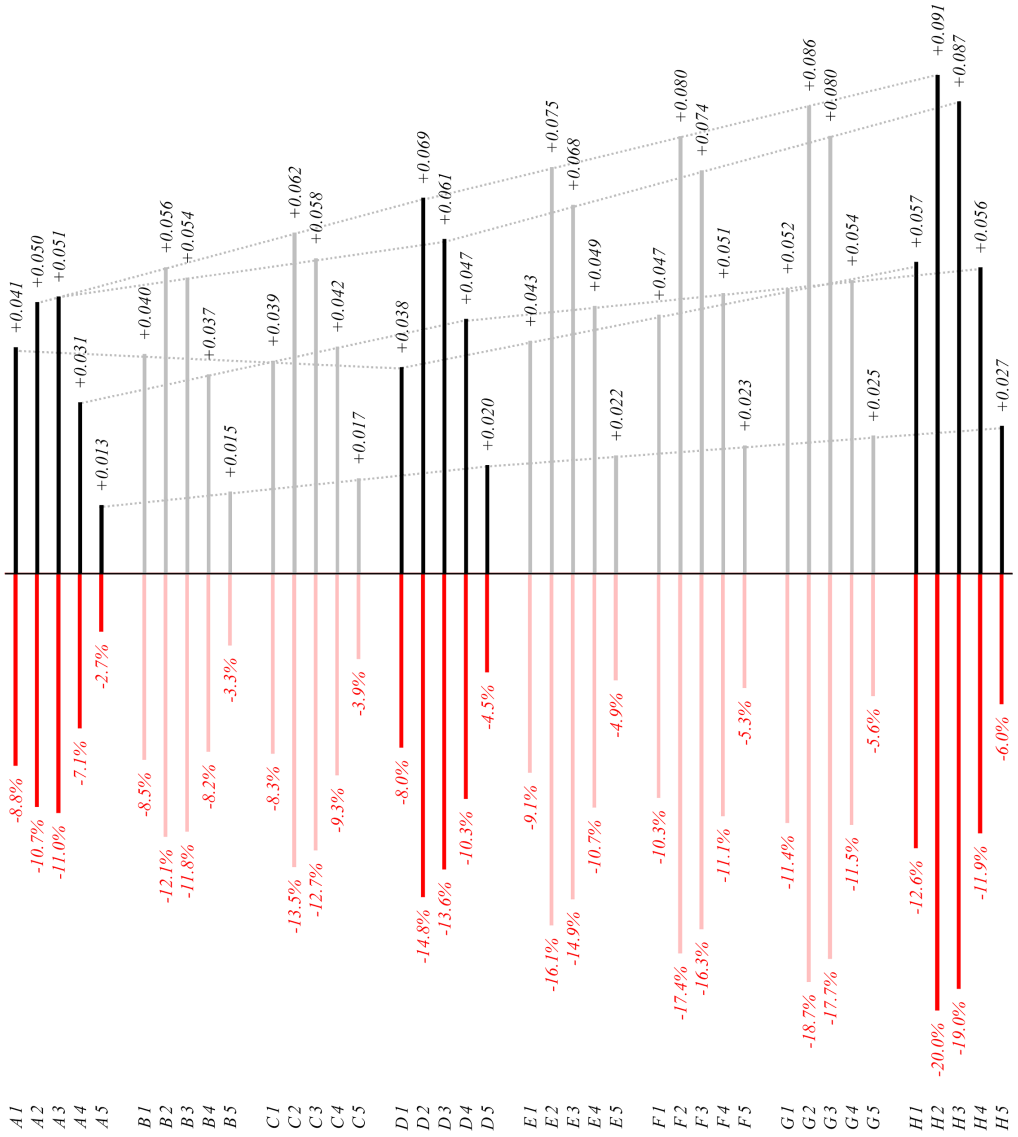

FIGURE 8. Histogram of mean changes in $c_{pe,\mathrm{mean}}$ on the windward faces of the ruin model.

The largest value of change $c_{pe,\mathrm{mean}}$ +0.052 (+26.7 %) is induced by alternative H1.

Figure 8 shows a histogram of mean changes in $c_{pe,\mathrm{mean}}$ values on the leeward surfaces of the ruin model surface. Observed values do not confirm the previous development pattern that larger changes are induced by roofs in contact with the ruin – the greatest changes are observed in alternative 2, which is 0.5 meters off the crown of the masonry (or alternative 3 in case of the branch A, but with only a small difference). H2 alternative caused the largest value of change in $c_{pe,\mathrm{mean}}$ +0.091 (−20.0 %).

Figure 9 shows a histogram of mean changes in $c_{f,\mathrm{mean}}$ values on the entire surface of the ruin model. According to alternatives 2–5, $c_{f,\mathrm{mean}}$ only increases between branches A–D. There is no significant effect on the values by increasing overlap size beyond branch D. There is an almost linear decline in the values depending on the size of the overlap in roof alternative 1. Compared to D and H, branch A has a different development pattern in value, based on offset size. Alternative 5 produces the greatest positive changes in branch A, while alternative 4 produces the greatest negative changes in branches D and H. The largest value of negative change $c_{f,\mathrm{mean}}$ -1.48×10^{-3} (−33.6 %) is caused by alternative H1, and positive change $+3.17 \times 10^{-4}$ (+8.0 %) by alternative D4 (very similar value to other 4 alternatives).

Figure 10 shows a histogram of mean changes in $c_{f,\mathrm{mean}}$ values on the ruin masonry head. The values increase in relation to the roof overlap size. The growth rate between branches A–D and D–H, however, differs. Branch A has a different character when it comes to the dependence of $c_{f,\mathrm{mean}}$ on the roof offset than branches D and H. Between alternatives 2 and 4 the change in $c_{f,\mathrm{mean}}$ increases and then decreases for branch A. For branches D, H, however, the change in $c_{f,\mathrm{mean}}$ is purely descending. The largest observed negative change in $c_{f,\mathrm{mean}}$ value -2.95×10^{-4} (−11.2 %) is caused by the roofing alternative A2, the largest positive change $+5.16 \times 10^{-3}$ (+83.3 %) by alternative H2.

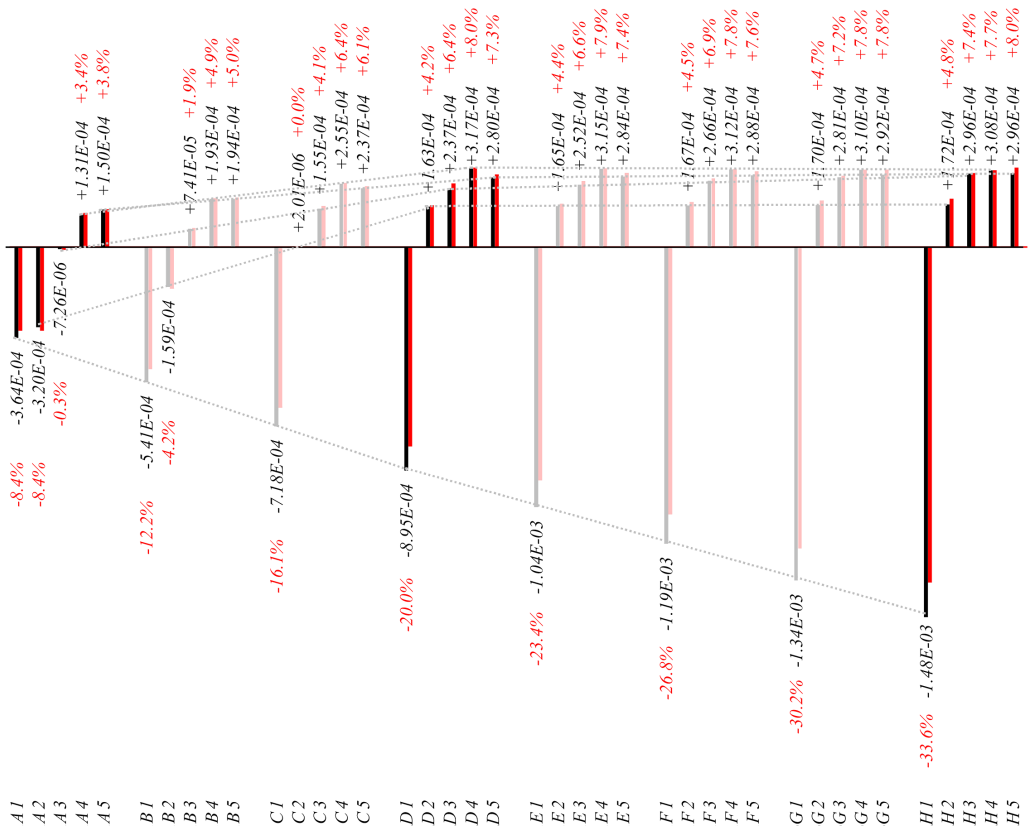

FIGURE 9. Histogram of mean changes in $c_{f,\mathrm{mean}}$ on the entire surface of ruin model.

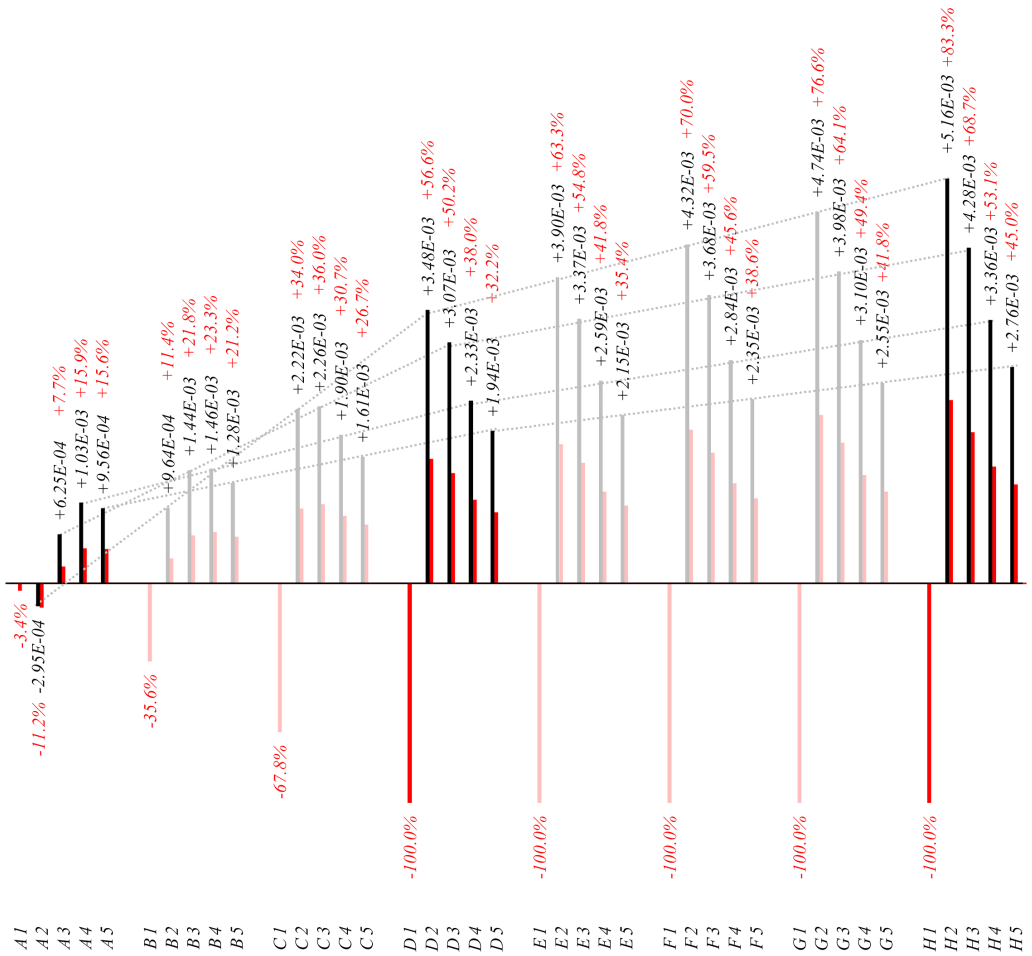

FIGURE 10. Histogram of mean changes in $c_{f,\mathrm{mean}}$ on the ruin masonry heads.

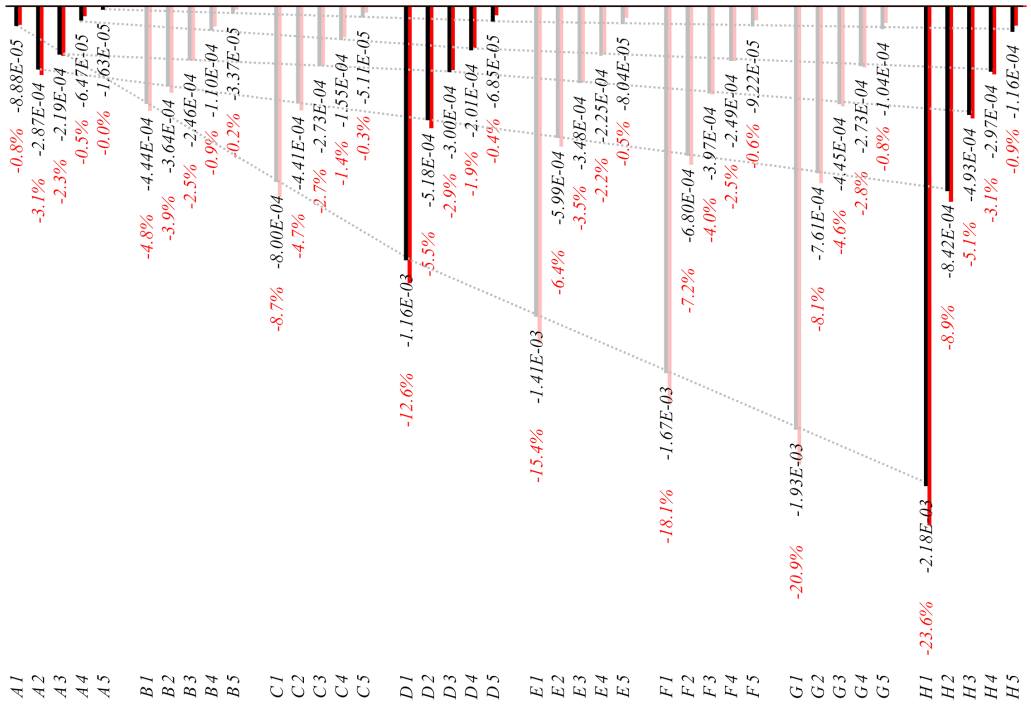

FIGURE 11. Histogram of mean changes in $c_{f,\mathrm{mean}}$ on the windward faces of the ruin model.

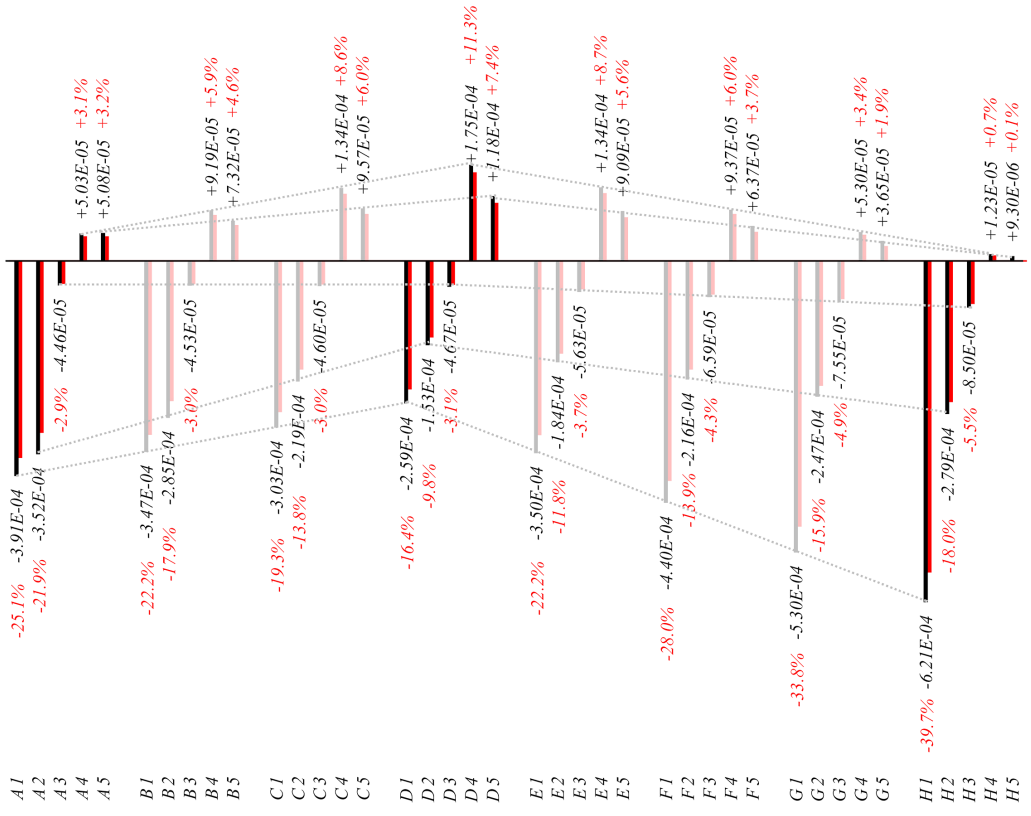

FIGURE 12. Histogram of mean changes in $c_{f,\mathrm{mean}}$ on the leeward faces of the ruin model.

Figure 11 shows a histogram of mean changes in $c_{f,\mathrm{mean}}$ values on windward surfaces of the ruin model surface. All monitored values are negative and have a related decreasing character in the direction of branches A–H and alternatives 1–5, apart from the direct contact roof alternative A1, which causes smaller negative changes than the following alternative A2 with a slight offset of the roof from the ruin. When a certain value is reached, the effect of the roof offset from the ruin on the change in $c_{f,\mathrm{mean}}$ values vanishes. The largest negative change of -2.18×10^{-3} ($-23.6\,\%$) is observed for roofing alternative H1.

Figure 12 shows a histogram of mean changes in $c_{f,\mathrm{mean}}$ values on the leeward surfaces of the

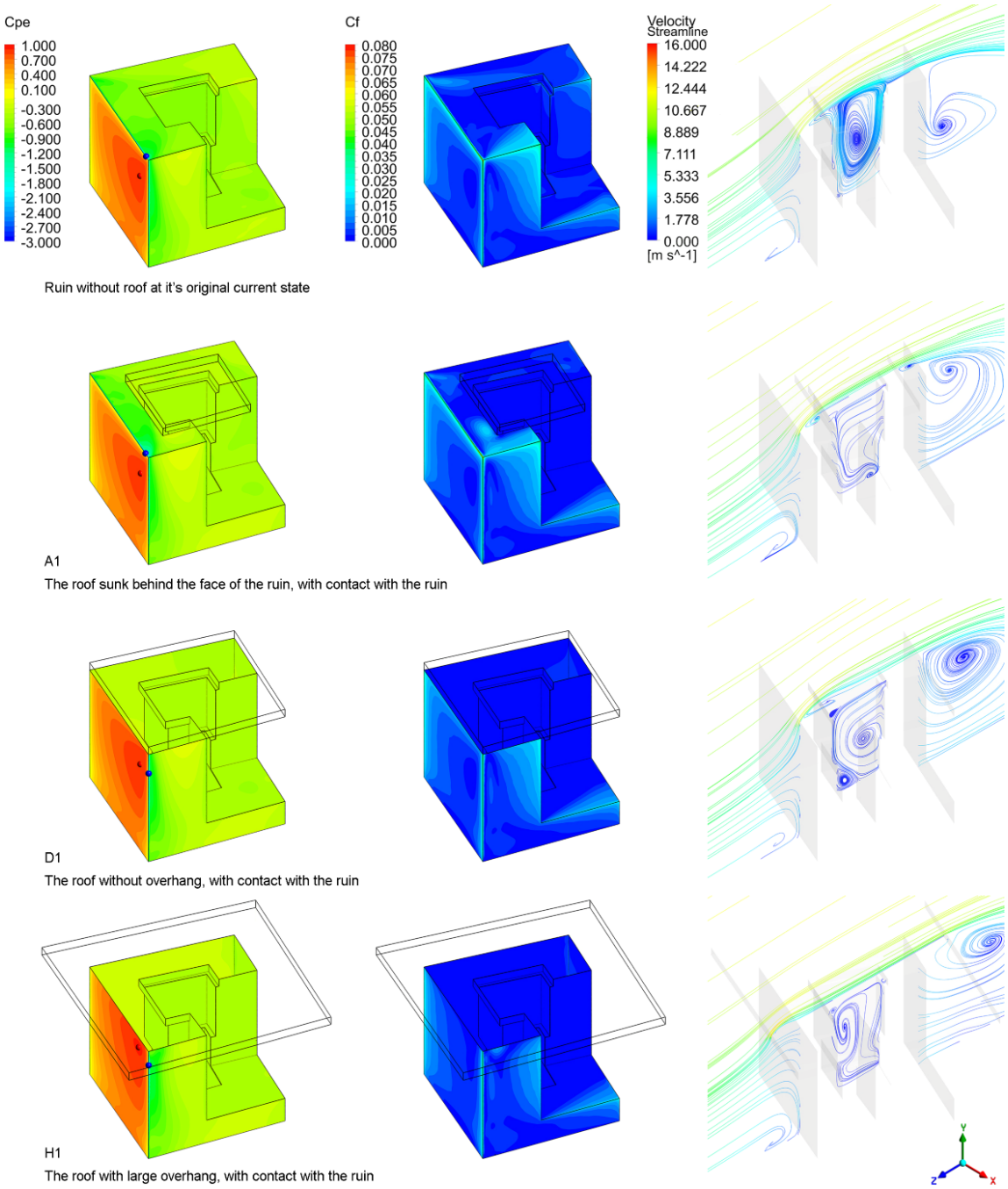

FIGURE 13. 3D illustration of external pressure coefficient $c_{pe,\mathrm{mean}}$ distribution, skin friction coefficient $c_{f,\mathrm{mean}}$ distribution, and streamlines at middle vertical plane.

ruin model surface. Value changes increase between branches A–D (except for alternative 3, for which they are almost constant) and decrease between branches D–H. The largest positive change $+1.75 \times 10^{-4}$ (+11.3 %) is observed for the roofing alternative D4, the largest negative change -6.21×10^{-4} (−39.7 %) for the alternative H1.

4. DISCUSSION

Changes in $c_{pe,\mathrm{mean}}$ and $c_{f,\mathrm{mean}}$ are calculated from averaging the changes observed in the three selected flow directions. The nature of the change development as a function of the roof offset and overhang sizes is derived from the flow simulation around selected three of the eight branches, set by the matrix of alternatives.

When trying to evaluate the optimal roofing alternative from the point of view of the changes in the values of the observed coefficients, it is critical to remember the baseline values of the coefficients in the initial state of the ruin without roofing. The shift towards zero is generally considered to be a positive change, so positive change in $c_{pe,\mathrm{mean}}$ values are preferred on the entire surface, the masonry head and leeward faces, where the original $c_{pe,\mathrm{mean}}$ is negative. In windward faces, when the original $c_{pe,\mathrm{mean}}$ reaches positive values, negative changes in value are preferred. From

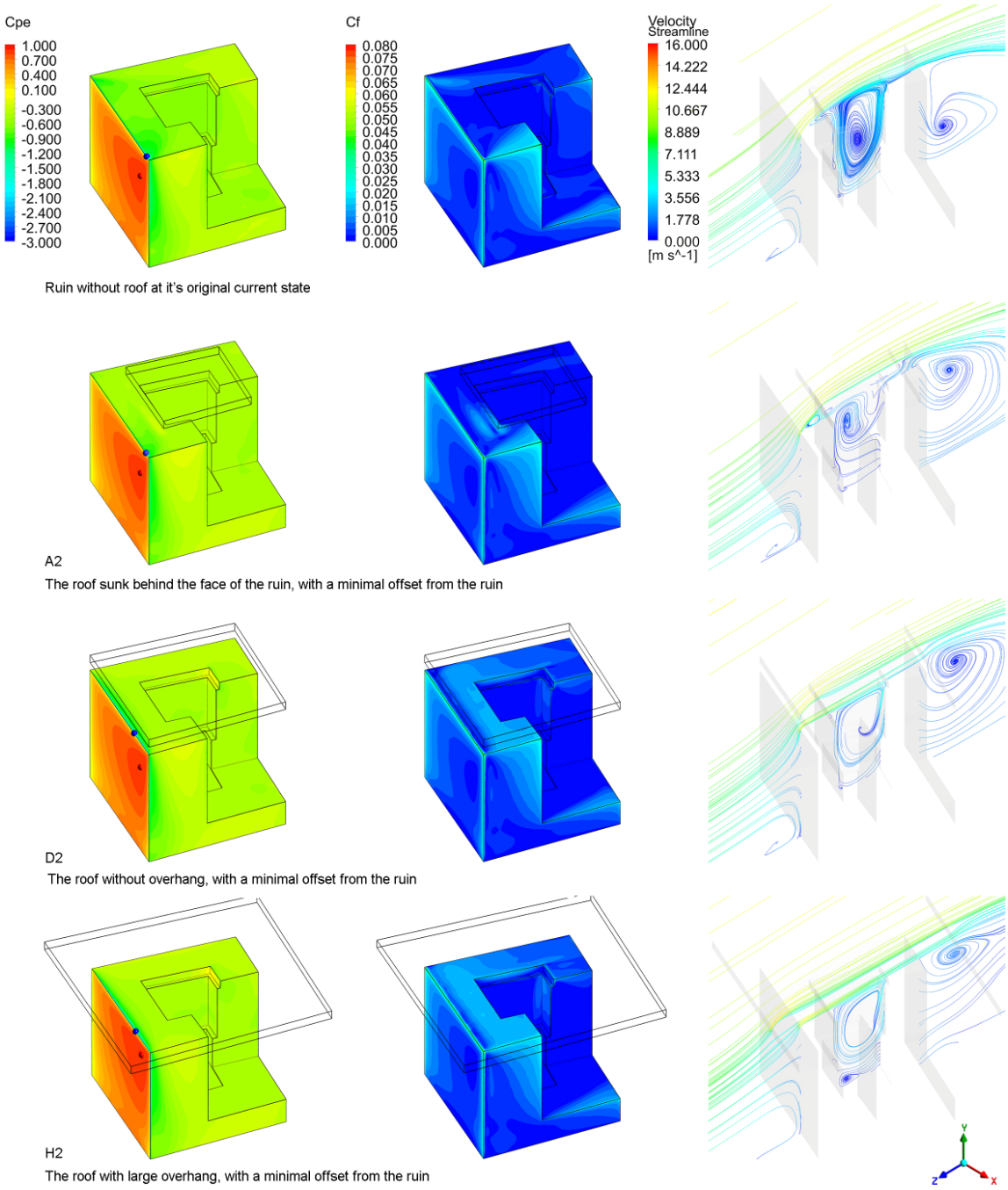

FIGURE 14. 3D illustration of external pressure coefficient $c_{pe,\mathrm{mean}}$ distribution, skin friction coefficient $c_{f,\mathrm{mean}}$ distribution, and streamlines at middle vertical plane.

the point of view of observed $c_{f,\mathrm{mean}}$ values, negative changes are evaluated as positive.

From the point of view of the $c_{pe,\mathrm{mean}}$ values on the entire surface of the ruin model, the roofing alternatives with direct contact with the ruin with as much overlap as possible appear to be more suitable, even though they worsen values on the windward faces and do not cause the greatest positive changes on the leeward faces. From the perspective of $c_{f,\mathrm{mean}}$ values, the suitability of such roofing alternatives is confirmed.

From the stance of $c_{pe,\mathrm{mean}}$ values, alternatives placed as close to the masonry head with as much overhang as possible appear to be more suitable when direct contact with the ruin is methodologically undesirable. However, these alternatives may be controversial from the perspective of $c_{f,\mathrm{mean}}$ values over the entire ruin surface, particularly on the masonry head, where a significant increase in values is observed. This phenomenon has been attributed to the manipulation of flow directions between the head and the roof, where the streamlines take a parallel path, see Figures 13 and 14. Thus, this study did not identify an ideal alternative of roof without direct contact with the ruin.

By adding more flow directions and roof alternative branches, the observed values and the development

patterns of the monitored coefficients could be verified. Including branches B and C in the simulations would clarify the changes between maximum embedment and zero overhang of the roof, as the A branch show patterns different to branches D and H. It might prove beneficial to also include intermediate values of the roof offset between alternatives 1 with direct contact and 2 with the offset size of 0.5 m, since these alternatives are most likely to exhibit atypical development patterns. Simulation of other shapes and types of covering roof would be beneficial in quantification of overhang and distance of the roof as protective design parameters.

5. Conclusion

The paper presented the effect of the offset and overhang of the board body over the ruin, representing the construction of a flat roof, on the changes in the mean values of external pressure coefficient c_{pe} and the surface friction coefficient c_f on the entire surface of the selected ruin model, the masonry head, windward and leeward faces. There was a 0.5 m gradually increasing distance between the roof and the ruin, calculated as a quarter of its masonry thickness. In the monitored coefficients, two noticeable changes were observed – those with large overhangs and close to the ruin showed the most significant changes. Two interesting roofing alternatives were determined. The first one is the alternative with direct contact with the ruin and the largest overhang, which caused the largest positively evaluated change in $c_{pe,\mathrm{mean}}$ value over the entire surface of the ruin model, even though it produced a negatively evaluated change in $c_{pe,\mathrm{mean}}$ value on the windward side. The second one is with a close offset from the ruin and the largest overlap, which caused the greatest positive change in $c_{pe,\mathrm{mean}}$ value on the leeward faces, but a negative change in $c_{f,\mathrm{mean}}$ value on the masonry head.

Acknowledgements

As part of the Program for Young Researchers Support at the Slovak University of Technology in Bratislava, the equipment for the construction of a physical idealized ruin model was purchased through the project Simulation of the impact of the shape of the roof over the ruin on the distribution of wind pressure in critical areas (BOREAS). A physical model of the ruin was created on the 3D printers at the Department of Architecture of the Faculty of Architecture of the Slovak University of Technology in Bratislava, which was acquired with the support of the Penta Foundation.

The research presented in this scientific paper is supported by the Ministry of Education, Science, Research and Sport of the Slovak republic, by the project VEGA 1/0322/23.

References

[1] O. Makýš. *Technológia obnovy budov: Realizácia obnovy kultúrnych pamiatok [In Slovak; Technology of building renovation: Implementation of renovation of cultural monuments]*. Spektrum STU, Slovak Republic, 2018. ISBN 978-80-227-4880-3.

[2] C. How. *Conservation of Ruins*, chap. Stability and survival, pp. 10–43. Butterworth-Heinermann, United Kingdom, 1st edn., 2007. ISBN 978-0-75-066429-5.

[3] E. Sesana, A. S. Gagnon, C. Ciantelli, et al. Climate change impacts on cultural heritage: A literature review. *WIREs Climate Change* **12**(4):e710, 2021. https://doi.org/10.1002/wcc.710

[4] C. Sabbioni, P. Brimblecombe, M. Cassar. *The atlas of climate change impact on European cultural heritage: Scientific analysis and management strategies*. Anthem Press, United Kingdom, 2010. ISBN 978-92-79-09800-0. https://doi.org/10.2777/11959

[5] M. Shao, L. Li, S. Wang, et al. Deterioration mechanisms of building materials of Jiaohe ruins in China. *Journal of Cultural Heritage* **14**(1):38–44, 2013. https://doi.org/10.1016/j.culher.2012.03.006

[6] E. Vojteková, J. Gregorová, B. Polomová, K. Sásiková. Monument restoration – a controlled task does not limit creativity. *World Transactions on Engineering and Technology Education* **16**(3):269–274, 2018.

[7] J. Gregorová, L. Chovancová, Z. Ondrejková, A. Škrinárová. Obnova torz architektúry ako špecializovaná architektonická disciplína [In Slovak; Restoration of ruins of architecture as a specialized architectural discipline]. *Archaeologia historica* **40**(1):7–39, 2015. https://doi.org/10.5817/AH2015-1-1

[8] B. Bielek, M. Franek, M. Bielek. *Aerodynamika a hydrodynamika budov: Fyzikálne problémy účinku vetra a hnaného dažďa na budovy a konštrukcie [In Slovak; Aerodynamics and hydrodynamics of building: Physics issues of wind effect and wind-driven rain on buildings and constructions]*. Spektrum STU, Slovak Republic, 2020. ISBN 978-80-227-5051-6.

[9] J. Singh, A. K. Roy. Effects of roof slope and wind direction on wind pressure distribution on the roof of a square plan pyramidal low-rise building using CFD simulation. *International Journal of Advanced Structural Engineering* **11**(2):231–254, 2019. https://doi.org/10.1007/s40091-019-0227-3

[10] N. S. Fouad, G. H. Mahmoud, N. E. Nasr. Comparative study of international codes wind loads and CFD results for low rise buildings. *Alexandria Engineering Journal* **57**(4):3623–3639, 2018. https://doi.org/10.1016/j.aej.2017.11.023

[11] B. Mou, B.-J. He, D.-X. Zhao, K.-W. Chau. Numerical simulation of the effects of building dimensional variation on wind pressure distribution. *Engineering Applications of Computational Fluid Mechanics* **11**(1):293–309, 2017. https://doi.org/10.1080/19942060.2017.1281845

[12] C. Cabello-Briones, S. Mayorga-Pinilla, D. Vázquez-Moliní. Particulate dry deposition on sheltered archaeological remains: Considerations based on Complutum, a Roman site in Spain. *Journal of Cultural Heritage* **46**:218–225, 2020. https://doi.org/10.1016/j.culher.2020.07.005

[13] G. Carbonara. Protective shelters for archaeological sites: Proceedings of a symposium. *Conservation and Management of Archaeological Sites* **21**(4):282–291, 2019. https://doi.org/10.1080/13505033.2020.1794593

[14] F. J. Soria, L. F. Guerrero, A. B. García. Protective roof systems for archeological sites in Mexico. In *WIT Transactions on the Built Environment*, vol. 171, pp. 225–236. WITPress, 2017. https://doi.org/10.2495/STR170201

[15] F. Y. Çetin, B. Ipekoğlu. Impact of transparency in the design of protective structures for conservation of archaeological remains. *Journal of Cultural Heritage* **14**(3):e21–e24, 2013. https://doi.org/10.1016/j.culher.2012.10.019

[16] P. Pineda, A. Iranzo. Analysis of sand-loaded air flow erosion in heritage sites by computational fluid dynamics: Method and damage prediction. *Journal of Cultural Heritage* **25**:75–86, 2017. https://doi.org/10.1016/j.culher.2016.12.005

[17] A. S. Hussein, H. El-Shishiny. Wind flow modeling and simulation over the Giza plateau cultural heritage site in Egypt. *Journal on Computing and Cultural Heritage* **2**(2):6, 2009. https://doi.org/10.1145/1613672.1613674

[18] M. Vecco. Genius loci as a meta-concept. *Journal of Cultural Heritage* **41**:225–231, 2020. https://doi.org/10.1016/j.culher.2019.07.001

[19] M. Antrop. Sustainable landscapes: Contradiction, fiction or utopia? *Landscape and Urban Planning* **75**(3–4):187–197, 2006. https://doi.org/10.1016/j.landurbplan.2005.02.014

[20] L. D'Acci. A new type of cities for liveable futures: Isobenefit urbanism morphogenesis. *Journal of Environmental Management* **246**:128–140, 2019. https://doi.org/10.1016/j.jenvman.2019.05.129

[21] Z. Nádaská, P. Pilař. Conceptual solution for the revitalization of public spaces in Slovak towns: Case study Stupava. In *9. Architektura v perspektivě*, pp. 177–180. Vysoká škola báňská – Technická univerzita Ostrava, Czech Republic, 2017. ISBN 978-80-248-4058-1.

[22] R. Ruhig. Konzervácia historických prvkov aplikáciou zimných záhrad na fasáde bytového domu v Madride [In Slovak; Preservation of historic elements by application winter gardens on the facade of a residential building in Madrid]. In *9. Architektura v perspektivě*, pp. 254–255. Vysoká škola báňská – Technická univerzita Ostrava, Czech Republic, 2017. ISBN 978-80-248-4058-1.

[23] F. Bránický, J. Gregorová. Hľadanie stratenej identity oravského vidieka [In Slovak; Searching for lost identity of Orava countryside]. In *14. Architektura v perspektivě*, pp. 84–89. Vysoká škola báňská – Technická univerzita Ostrava, Czech Republic, 2022.

[24] J. Gregorová, E. Vojteková. Príprava komplexnej obnovy NKP mestského opevnenia v Trnave: Pilotný projekt katedry UNESCO pre obnovu architektonického dedičstva na STU v Bratislave (1. etapa) [In Slovak; Preparation of complex renovation of national cultural monument of the fortification of the town Trnava: Pilot project of the UNESCO chair for preservation of architectural heritage at Slovak university of technology in Bratislava (1st phase)], 2022. [2023-03-05]. https://www.archinfo.sk/diskusia/blog/diela/priprava-komplexnej-obnovy-nkp-mestskeho-opevnenia-v-trnave-pilotny-projekt-katedry-unesco-pre-obnovu-architektonickeho-dedicstva-na-stu-v-bratislave-1-etapa.html

[25] M. Poliak. Climatic exposure of Slovak ruins. In *Advances in Architectural, Civil and Environmental Engineering*, pp. 382–387. Spektrum STU, Slovak Republic, 2021. ISBN 978-80-227-5150-6.

[26] M. Poliak. Analýza geometrie styku ruiny so zastrešením [In Slovak; Geometry analysis of ruin-coverage contact]. In *Advances in Architectural, Civil and Environmental Engineering*, pp. 365–372. Spektrum STU, Slovak Republic, 2022. ISBN 97-80-227-5251-0.

[27] M. Poliak, J. Gregorová. Dopad zastrešenia ruiny na metodiku jej prezentácie vo vzťahu k exponovanosti [In Slovak; Impact of ruin coverage on presentation of the ruin in relation to exposition]. In *14. Architektura v perspektivě*, pp. 179–183. Vysoká škola báňská – Technická univerzita Ostrava, Czech Republic, 2022. ISBN 978-80-248-4646-0.

[28] J. Franke, A. Baklanov. *Best practice guideline for the CFD simulation of flows in the urban environment: COST action 732 quality assurance and improvement of microscale meteorological models*. COST Office, 2007.

[29] M. Poliak, M. Franek, J. Gregorová. Evaluation of a measurement turbulence model of the wind pressure on the ruin of a fortified tower. *Slovak Journal of Civil Engineering* **31**(2):25–36, 2023. https://doi.org/10.2478/sjce-2023-0010

[30] CFD Online. Skin friction coefficient. [2023-04-15]. https://www.cfd-online.com/Wiki/Skin_friction_coefficient

Appendix A.

	$c_{pe,\mathrm{mean},22.5°}$				$c_{pe,\mathrm{mean},247.5°}$				$c_{pe,\mathrm{mean},315°}$			
	Head	**WW**	**LW**	**ES**	**Head**	**WW**	**LW**	**ES**	**Head**	**WW**	**LW**	**ES**
-	−0.601	0.151	−0.485	−0.327	−0.601	0.159	−0.486	−0.33	−0.657	0.302	−0.4	−0.187
A1	−0.631	0.165	−0.432	−0.286	−0.605	0.17	−0.434	−0.286	−0.575	0.319	−0.381	−0.151
A2	−0.502	0.175	−0.427	−0.272	−0.503	0.185	−0.427	−0.273	−0.502	0.315	−0.368	−0.147
A3	−0.566	0.165	−0.437	−0.289	−0.56	0.174	−0.419	−0.277	−0.53	0.307	−0.363	−0.149
A4	−0.597	0.154	−0.466	−0.313	−0.586	0.165	−0.455	−0.306	−0.574	0.314	−0.356	−0.149
A5	−0.601	0.152	−0.469	−0.316	−0.593	0.156	−0.471	−0.318	−0.612	0.307	−0.394	−0.175
D1	0	0.201	−0.431	−0.241	0	0.199	−0.441	−0.252	0	0.348	−0.386	−0.1
D2	−0.496	0.176	−0.413	−0.263	−0.488	0.188	−0.397	−0.252	−0.414	0.327	−0.355	−0.125
D3	−0.579	0.166	−0.436	−0.289	−0.564	0.18	−0.416	−0.275	−0.468	0.324	−0.335	−0.122
D4	−0.612	0.163	−0.456	−0.306	−0.585	0.174	−0.425	−0.284	−0.519	0.318	−0.351	−0.138
D5	−0.623	0.152	−0.472	−0.32	−0.608	0.158	−0.47	−0.319	−0.559	0.313	−0.37	−0.154
H1	0	0.197	−0.489	−0.279	0	0.203	−0.369	−0.2	0	0.368	−0.342	−0.066
H2	−0.474	0.184	−0.394	−0.246	−0.468	0.193	−0.385	−0.241	−0.327	0.355	−0.318	−0.086
H3	−0.543	0.168	−0.408	−0.267	−0.528	0.191	−0.387	−0.25	−0.392	0.345	−0.316	−0.095
H4	−0.595	0.159	−0.443	−0.297	−0.541	0.189	−0.385	−0.251	−0.499	0.328	−0.374	−0.145
H5	−0.614	0.157	−0.461	−0.311	−0.609	0.163	−0.458	−0.31	−0.527	0.321	−0.371	−0.149

TABLE 6. Table with $c_{pe,\mathrm{mean}}$ values for three selected flow directions.

	$c_{pe,\mathrm{mean},22.5°,\mathrm{diff}} = c_{pe,\mathrm{mean},22.5°,N} - c_{pe,\mathrm{mean},22.5°}$							
	Head		**Windward**		**Leeward**		**Entire Surface**	
A1	−0.03	5 %	0.015	10 %	0.053	−11 %	0.041	−13 %
A2	0.099	−17 %	0.024	16 %	0.058	−12 %	0.054	−17 %
A3	0.035	−6 %	0.014	9 %	0.048	−10 %	0.038	−12 %
A4	0.005	−1 %	0.003	2 %	0.02	−4 %	0.014	−4 %
A5	0.001	0 %	0.002	1 %	0.016	−3 %	0.011	−3 %
D1	0.601	−100 %	0.05	33 %	0.054	−11 %	0.086	−26 %
D2	0.106	−18 %	0.025	17 %	0.073	−15 %	0.064	−20 %
D3	0.022	−4 %	0.015	10 %	0.049	−10 %	0.038	−12 %
D4	−0.011	2 %	0.013	8 %	0.029	−6 %	0.021	−6 %
D5	−0.021	4 %	0.002	1 %	0.013	−3 %	0.007	−2 %
H1	0.601	−100 %	0.046	31 %	−0.004	1 %	0.047	−14 %
H2	0.127	−21 %	0.033	22 %	0.091	−19 %	0.08	−25 %
H3	0.058	−10 %	0.018	12 %	0.077	−16 %	0.059	−18 %
H4	0.006	−1 %	0.009	6 %	0.042	−9 %	0.029	−9 %
H5	−0.013	2 %	0.006	4 %	0.024	−5 %	0.016	−5 %

TABLE 7. Whole and percentual differences between the $c_{pe,\mathrm{mean}}$ values on the surface of the alternatively roofed ruin model and model without roof for flow direction 22.5°.

	$c_{pe,\mathrm{mean},247.5°,\mathrm{diff}} = c_{pe,\mathrm{mean},247.5°,N} - c_{pe,\mathrm{mean},247.5°}$							
	Head		**Windward**		**Leeward**		**Entire Surface**	
A1	−0.004	1 %	0.011	7 %	0.052	−11 %	0.043	−13 %
A2	0.098	−16 %	0.026	16 %	0.06	−12 %	0.056	−17 %
A3	0.041	−7 %	0.015	9 %	0.068	−14 %	0.052	−16 %
A4	0.016	−3 %	0.006	4 %	0.031	−6 %	0.024	−7 %
A5	0.008	−1 %	−0.003	−2 %	0.016	−3 %	0.011	−3 %
D1	0.601	−100 %	0.04	25 %	0.046	−9 %	0.078	−24 %
D2	0.113	−19 %	0.029	18 %	0.089	−18 %	0.077	−23 %
D3	0.037	−6 %	0.021	13 %	0.071	−15 %	0.055	−17 %
D4	0.016	−3 %	0.015	10 %	0.062	−13 %	0.046	−14 %
D5	−0.007	1 %	−0.001	−1 %	0.017	−3 %	0.011	−3 %
H1	0.601	−100 %	0.044	28 %	0.118	−24 %	0.13	−39 %
H2	0.134	−22 %	0.034	21 %	0.101	−21 %	0.088	−27 %
H3	0.073	−12 %	0.032	20 %	0.099	−20 %	0.08	−24 %
H4	0.06	−10 %	0.03	19 %	0.101	−21 %	0.079	−24 %
H5	−0.007	1 %	0.004	2 %	0.029	−6 %	0.019	−6 %

TABLE 8. Whole and percentual differences between the $c_{pe,\mathrm{mean}}$ values on the surface of the alternatively roofed ruin model and model without roof for flow direction 247.5°.

	$c_{pe,\mathrm{mean},315°,\mathrm{diff}} = c_{pe,\mathrm{mean},315°,N} - c_{pe,\mathrm{mean},315°}$							
	Head		**Windward**		**Leeward**		**Entire Surface**	
A1	0.083	−13 %	0.017	6 %	0.019	−5 %	0.036	−19 %
A2	0.155	−24 %	0.013	4 %	0.031	−8 %	0.04	−21 %
A3	0.127	−19 %	0.005	2 %	0.036	−9 %	0.037	−20 %
A4	0.084	−13 %	0.012	4 %	0.043	−11 %	0.038	−20 %
A5	0.045	−7 %	0.004	1 %	0.006	−1 %	0.011	−6 %
D1	0.657	−100 %	0.046	15 %	0.014	−3 %	0.086	−46 %
D2	0.243	−37 %	0.025	8 %	0.045	−11 %	0.061	−33 %
D3	0.189	−29 %	0.022	7 %	0.064	−16 %	0.065	−35 %
D4	0.138	−21 %	0.016	5 %	0.049	−12 %	0.049	−26 %
D5	0.098	−15 %	0.011	3 %	0.03	−7 %	0.032	−17 %
H1	0.657	−100 %	0.066	22 %	0.057	−14 %	0.121	−65 %
H2	0.331	−50 %	0.053	18 %	0.082	−20 %	0.101	−54 %
H3	0.266	−40 %	0.043	14 %	0.084	−21 %	0.092	−49 %
H4	0.159	−24 %	0.026	9 %	0.025	−6 %	0.042	−22 %
H5	0.131	−20 %	0.019	6 %	0.028	−7 %	0.038	−20 %

TABLE 9. Whole and percentual differences between the $c_{pe,\mathrm{mean}}$ values on the surface of the alternatively roofed ruin model and model without roof for flow direction 315°.

$$c_{pe,\mathrm{mean,mean\_diff}} = \frac{c_{pe,\mathrm{mean},22.5^\circ,N} + c_{pe,\mathrm{mean},247.5^\circ,N} + c_{pe,\mathrm{mean},315^\circ}}{3}$$

	Head		Windward		Leeward		Entire Surface	
A1	0.016	−2 %	0.014	7 %	0.041	−9 %	0.04	−15 %
A2	0.118	−19 %	0.021	12 %	0.05	−11 %	0.05	−18 %
A3	0.068	−11 %	0.012	7 %	0.051	−11 %	0.042	−16 %
A4	0.035	−5 %	0.007	3 %	0.031	−7 %	0.025	−11 %
A5	0.018	−3 %	0.001	0 %	0.013	−3 %	0.011	−4 %
D1	0.62	−100 %	0.045	25 %	0.038	−8 %	0.084	−32 %
D2	0.154	−24 %	0.026	14 %	0.069	−15 %	0.068	−25 %
D3	0.083	−13 %	0.019	10 %	0.061	−14 %	0.053	−21 %
D4	0.048	−7 %	0.015	8 %	0.047	−10 %	0.038	−15 %
D5	0.023	−3 %	0.004	1 %	0.02	−5 %	0.016	−8 %
H1	0.62	−100 %	0.052	27 %	0.057	−13 %	0.099	−39 %
H2	0.197	−31 %	0.04	20 %	0.091	−20 %	0.09	−35 %
H3	0.132	−21 %	0.031	15 %	0.087	−19 %	0.077	−31 %
H4	0.075	−12 %	0.022	11 %	0.056	−12 %	0.05	−18 %
H5	0.037	−6 %	0.01	4 %	0.027	−6 %	0.024	−10 %

TABLE 10. Mean differences of $c_{pe,\mathrm{mean}}$ values on the surface of the alternatively roofed ruin model and model without roof.

	$c_{f,\mathrm{mean},22.5^\circ}$			
	Head	**Windward**	**Leeward**	**Entire surface**
-	5.83×10^{-3}	8.45×10^{-3}	1.67×10^{-3}	3.96×10^{-3}
A1	5.63×10^{-3}	8.47×10^{-3}	1.19×10^{-3}	3.60×10^{-3}
A2	4.35×10^{-3}	8.19×10^{-3}	9.61×10^{-4}	3.29×10^{-3}
A3	6.00×10^{-3}	8.36×10^{-3}	1.65×10^{-3}	3.95×10^{-3}
A4	6.72×10^{-3}	8.52×10^{-3}	1.76×10^{-3}	4.14×10^{-3}
A5	6.53×10^{-3}	8.53×10^{-3}	1.77×10^{-3}	4.12×10^{-3}
D1	-	7.34×10^{-3}	1.23×10^{-3}	3.08×10^{-3}
D2	9.44×10^{-3}	7.98×10^{-3}	1.45×10^{-3}	4.11×10^{-3}
D3	9.19×10^{-3}	8.46×10^{-3}	1.62×10^{-3}	4.31×10^{-3}
D4	8.47×10^{-3}	8.56×10^{-3}	1.85×10^{-3}	4.40×10^{-3}
D5	7.86×10^{-3}	8.64×10^{-3}	1.88×10^{-3}	4.37×10^{-3}
H1	-	6.38×10^{-3}	8.50×10^{-4}	2.53×10^{-3}
H2	1.13×10^{-2}	7.79×10^{-3}	1.35×10^{-3}	4.19×10^{-3}
H3	1.02×10^{-2}	8.12×10^{-3}	1.57×10^{-3}	4.31×10^{-3}
H4	9.27×10^{-3}	8.43×10^{-3}	1.70×10^{-3}	4.35×10^{-3}
H5	8.61×10^{-3}	8.53×10^{-3}	1.87×10^{-3}	4.42×10^{-3}

TABLE 11. $c_{f,\mathrm{mean}}$ values for flow direction 22.5°.

	$c_{f,\mathrm{mean},247.5^\circ}$			
	Head	**Windward**	**Leeward**	**Entire surface**
-	5.09×10^{-3}	8.51×10^{-3}	1.50×10^{-3}	3.75×10^{-3}
A1	5.22×10^{-3}	8.44×10^{-3}	9.72×10^{-4}	3.38×10^{-3}
A2	3.75×10^{-3}	8.19×10^{-3}	1.32×10^{-3}	3.41×10^{-3}
A3	5.48×10^{-3}	8.29×10^{-3}	1.42×10^{-3}	3.70×10^{-3}
A4	6.25×10^{-3}	8.58×10^{-3}	1.58×10^{-3}	3.96×10^{-3}
A5	6.50×10^{-3}	8.55×10^{-3}	1.58×10^{-3}	4.00×10^{-3}
D1	-	7.24×10^{-3}	1.28×10^{-3}	3.04×10^{-3}
D2	9.33×10^{-3}	8.03×10^{-3}	1.42×10^{-3}	4.06×10^{-3}
D3	8.79×10^{-3}	8.26×10^{-3}	1.60×10^{-3}	4.17×10^{-3}
D4	7.81×10^{-3}	8.29×10^{-3}	1.76×10^{-3}	4.17×10^{-3}
D5	7.64×10^{-3}	8.53×10^{-3}	1.70×10^{-3}	4.18×10^{-3}
H1	-	6.28×10^{-3}	7.53×10^{-4}	2.39×10^{-3}
H2	1.12×10^{-2}	7.74×10^{-3}	1.36×10^{-3}	4.15×10^{-3}
H3	1.01×10^{-2}	8.11×10^{-3}	1.46×10^{-3}	4.19×10^{-3}
H4	8.79×10^{-3}	8.07×10^{-3}	1.68×10^{-3}	4.17×10^{-3}
H5	8.57×10^{-3}	8.61×10^{-3}	1.64×10^{-3}	4.26×10^{-3}

TABLE 12. $c_{f,\mathrm{mean}}$ values for flow direction 247.5°.

	$c_{f,\mathrm{mean},315^\circ}$			
	Head	**Windward**	**Leeward**	**Entire surface**
-	1.06×10^{-2}	1.12×10^{-2}	1.48×10^{-3}	5.84×10^{-3}
A1	9.61×10^{-3}	1.09×10^{-2}	1.31×10^{-3}	5.48×10^{-3}
A2	1.26×10^{-2}	1.09×10^{-2}	1.32×10^{-3}	5.89×10^{-3}
A3	1.19×10^{-2}	1.08×10^{-2}	1.44×10^{-3}	5.88×10^{-3}
A4	1.17×10^{-2}	1.08×10^{-2}	1.46×10^{-3}	5.85×10^{-3}
A5	1.14×10^{-2}	1.10×10^{-2}	1.46×10^{-3}	5.88×10^{-3}
D1	-	1.01×10^{-2}	1.36×10^{-3}	4.75×10^{-3}
D2	1.32×10^{-2}	1.06×10^{-2}	1.32×10^{-3}	5.87×10^{-3}
D3	1.28×10^{-2}	1.05×10^{-2}	1.29×10^{-3}	5.78×10^{-3}
D4	1.23×10^{-2}	1.07×10^{-2}	1.57×10^{-3}	5.93×10^{-3}
D5	1.19×10^{-2}	1.07×10^{-2}	1.43×10^{-3}	5.84×10^{-3}
H1	-	8.91×10^{-3}	1.18×10^{-3}	4.19×10^{-3}
H2	1.46×10^{-2}	1.01×10^{-2}	1.11×10^{-3}	5.72×10^{-3}
H3	1.40×10^{-2}	1.04×10^{-2}	1.37×10^{-3}	5.93×10^{-3}
H4	1.36×10^{-2}	1.07×10^{-2}	1.31×10^{-3}	5.95×10^{-3}
H5	1.26×10^{-2}	1.06×10^{-2}	1.17×10^{-3}	5.75×10^{-3}

TABLE 13. $c_{f,\mathrm{mean}}$ values for flow direction 315°.

	$c_{f,\mathrm{mean},22.5^\circ,\mathrm{diff}} = c_{f,\mathrm{mean},22.5^\circ,N} - c_{f,\mathrm{mean},22.5^\circ}$							
	Head		**Windward**		**Leeward**		**Entire Surface**	
A1	-1.95×10^{-4}	−3 %	1.45×10^{-5}	0 %	-4.77×10^{-4}	−29 %	-3.59×10^{-4}	−9 %
A2	-1.48×10^{-3}	−25 %	-2.62×10^{-4}	−3 %	-7.07×10^{-4}	−42 %	-6.67×10^{-4}	−17 %
A3	1.74×10^{-4}	3 %	-9.31×10^{-5}	−1 %	-1.65×10^{-5}	−1 %	-1.08×10^{-5}	0 %
A4	8.90×10^{-4}	15 %	6.46×10^{-5}	1 %	9.60×10^{-5}	6 %	1.82×10^{-4}	5 %
A5	6.99×10^{-4}	12 %	7.44×10^{-5}	1 %	9.85×10^{-5}	6 %	1.63×10^{-4}	4 %
D1	-5.83×10^{-3}	−100 %	-1.12×10^{-3}	−13 %	-4.36×10^{-4}	−26 %	-8.84×10^{-4}	−22 %
D2	3.62×10^{-3}	62 %	-4.76×10^{-4}	−6 %	-2.17×10^{-4}	−13 %	1.47×10^{-4}	4 %
D3	3.36×10^{-3}	58 %	9.86×10^{-6}	0 %	-4.68×10^{-5}	−3 %	3.53×10^{-4}	9 %
D4	2.64×10^{-3}	45 %	1.05×10^{-4}	1 %	1.82×10^{-4}	11 %	4.41×10^{-4}	11 %
D5	2.04×10^{-3}	35 %	1.84×10^{-4}	2 %	2.10×10^{-4}	13 %	4.11×10^{-4}	10 %
H1	-5.83×10^{-3}	−100 %	-2.07×10^{-3}	−25 %	-8.17×10^{-4}	−49 %	-1.43×10^{-3}	−36 %
H2	5.44×10^{-3}	93 %	-6.65×10^{-4}	−8 %	-3.20×10^{-4}	−19 %	2.31×10^{-4}	6 %
H3	4.42×10^{-3}	76 %	-3.30×10^{-4}	−4 %	-9.95×10^{-5}	−6 %	3.50×10^{-4}	9 %
H4	3.45×10^{-3}	59 %	-2.60×10^{-5}	0 %	2.93×10^{-5}	2 %	3.95×10^{-4}	10 %
H5	2.78×10^{-3}	48 %	7.30×10^{-5}	1 %	2.04×10^{-4}	12 %	4.63×10^{-4}	12 %

TABLE 14. Whole and percentual differences between the $c_{f,\mathrm{mean}}$ values on the surface of the alternatively roofed ruin model and model without roof for flow direction 22.5°.

	$c_{f,\mathrm{mean},247.5^\circ,\mathrm{diff}} = c_{f,\mathrm{mean},247.5^\circ,N} - c_{f,\mathrm{mean},247.5^\circ}$							
	Head		**Windward**		**Leeward**		**Entire Surface**	
A1	1.33×10^{-4}	3 %	-6.92×10^{-5}	−1 %	-5.26×10^{-4}	−35 %	-3.69×10^{-4}	−10 %
A2	-1.34×10^{-3}	−26 %	-3.17×10^{-4}	−4 %	-1.82×10^{-4}	−12 %	-3.40×10^{-4}	−9 %
A3	3.89×10^{-4}	8 %	-2.12×10^{-4}	−2 %	-7.59×10^{-5}	−5 %	-4.66×10^{-5}	−1 %
A4	1.16×10^{-3}	23 %	6.86×10^{-5}	1 %	8.05×10^{-5}	5 %	2.06×10^{-4}	6 %
A5	1.42×10^{-3}	28 %	4.21×10^{-5}	0 %	8.05×10^{-5}	5 %	2.49×10^{-4}	7 %
D1	-5.09×10^{-3}	−100 %	-1.27×10^{-3}	−15 %	-2.21×10^{-4}	−15 %	-7.10×10^{-4}	−19 %
D2	4.24×10^{-3}	83 %	-4.79×10^{-4}	−6 %	-7.55×10^{-5}	−5 %	3.16×10^{-4}	8 %
D3	3.70×10^{-3}	73 %	-2.48×10^{-4}	−3 %	9.98×10^{-5}	7 %	4.24×10^{-4}	11 %
D4	2.73×10^{-3}	54 %	-2.18×10^{-4}	−3 %	2.61×10^{-4}	17 %	4.21×10^{-4}	11 %
D5	2.55×10^{-3}	50 %	2.76×10^{-5}	0 %	2.01×10^{-4}	13 %	4.31×10^{-4}	11 %
H1	-5.09×10^{-3}	−100 %	-2.23×10^{-3}	−26 %	-7.44×10^{-4}	−50 %	-1.36×10^{-3}	−36 %
H2	6.07×10^{-3}	119 %	-7.66×10^{-4}	−9 %	-1.42×10^{-4}	−9 %	4.01×10^{-4}	11 %
H3	5.00×10^{-3}	98 %	-3.98×10^{-4}	−5 %	-3.95×10^{-5}	−3 %	4.45×10^{-4}	12 %
H4	3.70×10^{-3}	73 %	-4.32×10^{-4}	−5 %	1.79×10^{-4}	12 %	4.23×10^{-4}	11 %
H5	3.48×10^{-3}	68 %	1.01×10^{-4}	1 %	1.41×10^{-4}	9 %	5.15×10^{-4}	14 %

TABLE 15. Whole and percentual differences between the $c_{f,\mathrm{mean}}$ values on the surface of the alternatively roofed ruin model and model without roof for flow direction 247.5°.

	$c_{f,\mathrm{mean},315^\circ,\mathrm{diff}} = c_{f,\mathrm{mean},315^\circ,N} - c_{f,\mathrm{mean},315^\circ}$							
	Head		**Windward**		**Leeward**		**Entire Surface**	
A1	-1.01×10^{-3}	−10 %	-2.12×10^{-4}	−2 %	-1.70×10^{-4}	−11 %	-3.63×10^{-4}	−6 %
A2	1.93×10^{-3}	18 %	-2.82×10^{-4}	−3 %	-1.66×10^{-4}	−11 %	4.66×10^{-5}	1 %
A3	1.31×10^{-3}	12 %	-3.52×10^{-4}	−3 %	-4.13×10^{-5}	−3 %	3.57×10^{-5}	1 %
A4	1.04×10^{-3}	10 %	-3.27×10^{-4}	−3 %	-2.55×10^{-5}	−2 %	6.22×10^{-6}	0 %
A5	7.52×10^{-4}	7 %	-1.65×10^{-4}	−1 %	-2.66×10^{-5}	−2 %	3.96×10^{-5}	1 %
D1	-1.06×10^{-2}	−100 %	-1.08×10^{-3}	−10 %	-1.21×10^{-4}	−8 %	-1.09×10^{-3}	−19 %
D2	2.59×10^{-3}	24 %	-5.99×10^{-4}	−5 %	-1.67×10^{-4}	−11 %	2.68×10^{-5}	0 %
D3	2.16×10^{-3}	20 %	-6.61×10^{-4}	−6 %	-1.93×10^{-4}	−13 %	-6.61×10^{-5}	−1 %
D4	1.62×10^{-3}	15 %	-4.89×10^{-4}	−4 %	8.28×10^{-5}	6 %	8.79×10^{-5}	2 %
D5	1.24×10^{-3}	12 %	-4.17×10^{-4}	−4 %	-5.62×10^{-5}	−4 %	-2.99×10^{-6}	0 %
H1	-1.06×10^{-2}	−100 %	-2.25×10^{-3}	−20 %	-3.01×10^{-4}	−20 %	-1.66×10^{-3}	−28 %
H2	3.96×10^{-3}	37 %	-1.09×10^{-3}	−10 %	-3.73×10^{-4}	−25 %	-1.17×10^{-4}	−2 %
H3	3.42×10^{-3}	32 %	-7.52×10^{-4}	−7 %	-1.16×10^{-4}	−8 %	9.19×10^{-5}	2 %
H4	2.93×10^{-3}	28 %	-4.33×10^{-4}	−4 %	-1.72×10^{-4}	−12 %	1.07×10^{-4}	2 %
H5	2.02×10^{-3}	19 %	-5.22×10^{-4}	−5 %	-3.17×10^{-4}	−21 %	-8.91×10^{-5}	−2 %

TABLE 16. Whole and percentual differences between the $c_{f,\mathrm{mean}}$ values on the surface of the alternatively roofed ruin model and model without roof for flow direction 315°.

	$c_{f,\mathrm{mean},\mathrm{mean\_diff}} = \frac{c_{f,\mathrm{mean},22.5^\circ,N} + c_{f,\mathrm{mean},247.5^\circ,N} + c_{f,\mathrm{mean},315^\circ}}{3}$							
	Head		**Windward**		**Leeward**		**Entire Surface**	
A1	-3.58×10^{-4}	−3 %	-8.88×10^{-5}	−1 %	-3.91×10^{-4}	−25 %	-3.64×10^{-4}	−8 %
A2	-2.95×10^{-4}	−11 %	-2.87×10^{-4}	−3 %	-3.52×10^{-4}	−22 %	-3.20×10^{-4}	−8 %
A3	6.25×10^{-4}	8 %	-2.19×10^{-4}	−2 %	-4.46×10^{-5}	−3 %	-7.26×10^{-6}	0 %
A4	1.03×10^{-3}	16 %	-6.47×10^{-5}	0 %	5.03×10^{-5}	3 %	1.31×10^{-4}	3 %
A5	9.56×10^{-4}	16 %	-1.63×10^{-5}	0 %	5.08×10^{-5}	3 %	1.50×10^{-4}	4 %
D1	-7.18×10^{-3}	−100 %	-1.16×10^{-3}	−13 %	-2.59×10^{-4}	−16 %	-8.95×10^{-4}	−20 %
D2	3.48×10^{-3}	57 %	-5.18×10^{-4}	−6 %	-1.53×10^{-4}	−10 %	1.63×10^{-4}	4 %
D3	3.07×10^{-3}	50 %	-3.00×10^{-4}	−3 %	-4.67×10^{-5}	−3 %	2.37×10^{-4}	6 %
D4	2.33×10^{-3}	38 %	-2.01×10^{-4}	−2 %	1.75×10^{-4}	11 %	3.17×10^{-4}	8 %
D5	1.94×10^{-3}	32 %	-6.85×10^{-5}	0 %	1.18×10^{-4}	7 %	2.80×10^{-4}	7 %
H1	-7.18×10^{-3}	−100 %	-2.18×10^{-3}	−24 %	-6.21×10^{-4}	−40 %	-1.48×10^{-3}	−34 %
H2	5.16×10^{-3}	83 %	-8.42×10^{-4}	−9 %	-2.79×10^{-4}	−18 %	1.72×10^{-4}	5 %
H3	4.28×10^{-3}	69 %	-4.93×10^{-4}	−5 %	-8.50×10^{-5}	−5 %	2.96×10^{-4}	7 %
H4	3.36×10^{-3}	53 %	-2.97×10^{-4}	−3 %	1.23×10^{-5}	1 %	3.08×10^{-4}	8 %
H5	2.76×10^{-3}	45 %	-1.16×10^{-4}	−1 %	9.30×10^{-6}	0 %	2.96×10^{-4}	8 %

TABLE 17. Mean differences of $c_{f,\mathrm{mean}}$ values on the surface of the alternatively roofed ruin model and model without roof.